Magnetic-field-induced recovery strain in polycrystalline Ni–Mn–Ga foam

Article *in* Journal of Applied Physics · December 2010

DOI: 10.1063/1.3524503

Magnetic-field-induced recovery strain in polycrystalline Ni–Mn–Ga foam

Markus Chmielus,[1,2,a)] Cassie Witherspoon,[1] Robert C. Wimpory,[3] Andreas Paulke,[3] André Hilger,[3] Xuexi Zhang,[4] David C. Dunand,[4] and Peter Müllner[1]
[1]*Department of Materials Science and Engineering, Boise State University, Boise, Idaho 83725, USA*
[2]*M-I1, Helmholtz Centre Berlin for Materials and Energy, Hahn-Meitner-Platz 1, 14109 Berlin, Germany*
[3]*F-I1, Helmholtz Centre Berlin for Materials and Energy, Hahn-Meitner-Platz 1, 14109 Berlin, Germany*
[4]*Department of Materials Science and Engineering, Northwestern University, Evanston, Illinois 60208, USA*

(Received 20 October 2010; accepted 1 November 2010; published online 30 December 2010)

Recently, we have shown that a polycrystalline Ni–Mn–Ga magnetic shape-memory alloy, when containing two populations of pore sizes, shows very high magnetic-field-induced strain of up to 8.7%. Here, this double-porosity sample is imaged by x-ray microtomography, showing a homogenous distribution of both pore populations. The orientation of six large grains—four with 10M and two with 14M structure—is identified with neutron diffraction. *In situ* magnetomechanical experiments with a rotating magnetic field demonstrate that strain incompatibilities between misoriented grains are effectively screened by the pores which also stop the propagation of microcracks. During uniaxial compression performed with an orthogonal magnetic bias field, a strain as high as 1% is recovered on unloading by twinning, which is much larger than the elastic value of $<0.1\%$ measured without field. At the same time, repeated loading and unloading results in a reduction in the yield stress, which is a training effect similar to that in single crystals.
 [doi:10.1063/1.3524503]

I. INTRODUCTION

Monocrystalline Ni–Mn–Ga magnetic shape-memory alloy (MSMA) show plastic and reversible magnetic-field-induced strains (MFISs) by the motion of twin boundaries (e.g., Ref. 1) of up to 10% (Refs. 2–4) nearly two orders of magnitude larger than commercially available magnetostrictive materials. The MFIS and high cycle performance of single crystalline MSMAs strongly depend on constraints, which may originate, e.g., from attaching the crystal to a sample holder.[5–7] These constraints lead to reduced MFIS and the formation of large twins in the regions close to the constraint surfaces. Large amounts of twinning dislocations pile up where large twins mutually interact and lead eventually to the formation of cracks and to failure by fracture.[6,7] Furthermore, the production and preparation of single crystalline MSMAs is difficult and time consuming.

Polycrystalline Ni–Mn–Ga shows vanishing small MFIS ($<0.01\%$ for small grains) because of internal constraints imposed by grain boundaries.[8–10] Internal constraints can be partially reduced when the material is strongly textured (e.g., by directional solidification) such that grains are oriented along one direction.[11] MSMAs with such a microstructure show considerable strain recovery of up to 1% upon unloading in a perpendicular magnetic bias field, particularly when exposed to mechanical training.[12] Constraints may also be partially reduced when the size of the material is in one or two dimensions less than the grain size, i.e., for thin films with columnar grain structure and in fibers and wires with bamboo grains.[13,14] For a fiber with bamboo grains spanning the whole section of the fiber, an MFIS of 1% was recently achieved.[14]

Reducing internal constraints by introduction of pores in the polycrystalline MSMA improves the MFIS significantly. For an open-pore foam with a monomodal pore size with 76% volume fraction, an MFIS of 0.12% was measured.[15] Much larger MFIS values of 2% were obtained for a foam with a bimodal pore size distribution[16] with 62% volume fraction. The MFIS was further increased to 8.7% with thermomagnetomechanical training, during which the porous MSMA was heated and cooled through the phase transformation while exposed to a rotating magnetic field. The mechanism reducing internal and external constraints via porosity and foam architecture is based on the reduction in twin-twin and twin-grain boundary interactions and is further discussed in Ref. 17.

In this study, we further study the same Ni–Mn–Ga polycrystalline foam for which an 8.7% MFIS was measured.[16] We observe optically the surface of the foam undergoing MFIS in a rotating magnetic field and confirm the hypothesis that large MFIS is indeed enabled by reducing of internal constraints with porosity. We then subject the foam to compressive deformation and measure a magnetic-field-induced recovery of up to 1% strain in an orthogonal magnetic bias field. We also analyze the pore architecture, the martensite structure, and the texture with x-ray microtomography and neutron diffraction.

II. EXPERIMENTAL PROCEDURES

The experiments were performed with the Ni–Mn–Ga foam sample with bimodal pore size distribution, for which up to 8.7% MFIS was previously measured in a rotating

[a)]Present address: Department of Materials Science and Engineering, Cornell University, 214 Bard Hall, Ithaca, NY 14853–1501, USA. Electronic mail: mc728@cornell.edu.

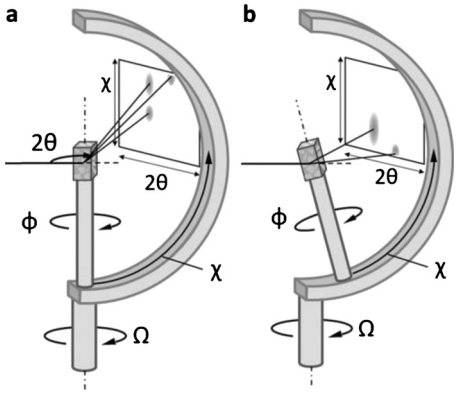

FIG. 1. Schematic of the neutron diffraction texture experiment at the E3 beamline of the Helmholtz Centre Berlin for Materials and Energy. (a) Shows a scan without tilting, $\chi=0°$ and (b) with the tilting step, $\chi=10°$. During the texture measurement operated in Ω mode, φ is kept constant for each χ step while the entire Euler cradle (with the sample) is rotated around Ω. The detector is spanning a χ and 2θ area of $12° \times 12°$.

magnetic field.[16] The foam, with atomic compositions $Ni_{52.9(5)}Mn_{23.9(5)}Ga_{23.2(5)}$, (measured with energy dispersive x-ray spectroscopy, values in parentheses indicate the estimated error) was created by liquid metal infiltration of a lightly sintered preform of sodium aluminate powders, followed by complete dissolution of the space-holder and partial dissolution of the metal resulting in an ingot with 62% porosity, which was then annealed in vacuum at 1000 °C for 1 h. Afterwards, the foam was subjected to a stepwise chemical ordering heat treatment (2 h at 725 °C, 10 h at 700 °C, and 20 h at 500 °C). A parallelepiped sample, with dimensions $x=2.3$ mm, $y=3.0$ mm, and $z=6.2$ mm, was cut from the ingot. Further details about foam and sample preparation are given in Ref. 16.

The pore distribution was characterized with x-ray microcomputer tomography. The x-ray radiation was generated by a microfocus tube (Hamamatsu, L8121-03) with a spot size of 7 μm and detected by a flat panel detector (Hamamatsu, C7942SK-05). The scanner was set to an acceleration voltage of 100 keV and a current of 95 μA. The out coming beam was filtered by a 1 mm thick Aluminum plate. The magnification ratio was preset to 7.1 with a effective pixel size of 7.1 μm for the sample. The reconstruction of the data set of 1000 projections was performed using OCTOPUS 8.3 software.

The martensite structure and texture were characterized with neutron diffraction at the E3 beamline of the Helmholtz Centre Berlin for Materials and Energy (HZB) using an Euler cradle and an area detector with 256×256 pixels[2]. E3 is a materials science and residual stress diffractomer used for solving a variety of engineering and material problems. The thermal neutron beam (1.486 Å wavelength) had a 6×6 mm^2 cross-section.[18] Figure 1 shows a schematic of the neutron diffraction experiment. In a first experiment [Fig. 1(a)] with constant $\chi=0°$, the sample was rotated with constant velocity around ϕ and the detector position was slowly and continuously changed to scan the 2θ range between 40° and 85°. In a second experiment [Fig. 1(b)], the sample was tilted around χ in 10° steps from 0° to 90°. At each χ step, the Euler cradle was rotated around Ω in 1/3° steps between

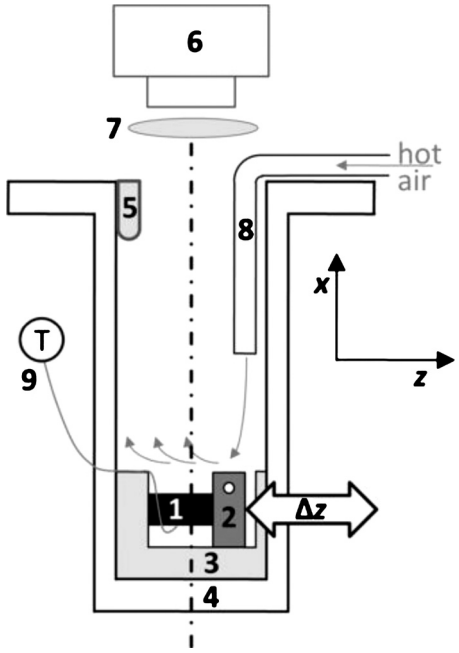

FIG. 2. Schematic of the modified magnetomechanical experiment. The foam (1) is glued to the sliding head (2) and holder (3). The sample holder is bolted to a tube (4), which is placed in the rotating field (field axis shown). An light emitting diode (5) is used to illuminate the foam surface, so that it can be observed with the optical camera (6). Different areas of the surface can be magnified with lenses (7). A tube (8) is used to direct heated and cooled air onto the sample. A thermocouple (9) measures the temperature on the foam surface. The dashed-dotted line marks the rotation axis of the magnetic field. The magnetic field vector is oriented perpendicular to the rotation axis.

0° and 180°. The detector was kept near constant during the entire test at $2\theta=95°$, spanning a small 2θ range from ~89° to 101°.

The magnetomechanical experiments were performed in a rotating magnetic field of 0.97 T with a test device described in detail in Ref. 16. To observe the MFIS *in situ* in the rotating field, this device was upgraded with an Infinity digital camera (Lumenera Corp, Ottawa, ON, Canada) with 21 megapixel resolution. To view the entire surface of the foam sample, the ceramic rod which is required to measure the MFIS digitally[16] was removed. The experimental setup is shown in Fig. 2. The foam itself was glued to the sample holder (no. 3 in Fig. 2) on one side and to a sliding head (no. 2 in Fig. 2) on the other side. While the sample holder is mounted firmly in the device, the sliding head is guided and can move in the z direction. The guidance limits motion in the y direction to ~10 μm. The sample chamber lid was not installed to allow optical observation. Self-lubricating Vespel® was used as sample chamber material to ensure minimum friction. During the test, the magnetic field was rotated at a uniform 30 rpm. The sample was heated with hot air from 16 to 35 °C within 3 min and then slowly cooled down by natural convection (without cold air as in Ref. 16, to avoid condensation on the camera lens).

After the sample was removed from the magnetomechanical test device, its magnetization was measured in all directions parallel to the y-z plane, using a Model 10 Vibrating Sample Magnetometer (with details given in Ref. 7). The sample was first measured in a magnetic field of 100 mT

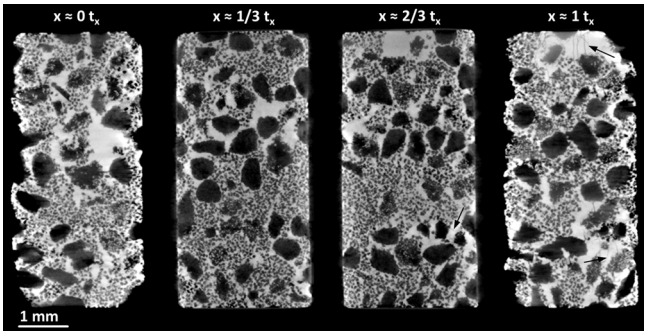

FIG. 3. X-ray tomography slices of the foam sample in the *y*-*z* plane along the *x* axis (parallel to the shortest dimension of the sample). t_x is the thickness of the sample in the *x* direction. Arrows indicate cracks.

while being rotated around its *x* axis. From this experiment, the easy and hard magnetization directions were identified and a saturation experiment was performed in these two directions by increasing the magnetic field from zero to 2 T. The magnetic field was corrected for the demagnetization factor.

Deformation experiments were performed in compression with and without orthogonal magnetic bias field with a model 1445 mechanical test bench (Zwick, Ulm, Germany) at a constant cross-head speed of 0.125 mm/min (see Ref. 19 for experimental details). During all tests, the load was applied parallel to the *z* direction of the sample. The sample was tested in three mechanical deformation cycles: in the first cycle without magnetic field during loading and unloading; in the second cycle without magnetic field during loading but with an orthogonal magnetic field of 1 T parallel to the *y* direction of the sample during unloading; and in the third cycle with a magnetic field of 1 T during both loading and unloading.

III. RESULTS

The x-ray tomography scans (Fig. 3) reveal a fairly homogenous distribution of both pore sizes throughout the entire sample. The center portion of the sample has a somewhat reduced number of large pores. Additionally, the cross section at $x \approx 2/3\ t_x$ and $x \approx t_x$ (where t_x is the thickness of the sample) showed small cracks in the bottom right regions and at $x \approx t_x$ also at the top edge of the sample. These cracks spanned between large pores and can also be seen between some small pores that are located between large pores (arrows in Fig. 3).

The results of the neutron diffraction experiments are shown in Figs. 4–6. In the first experiment which was performed at constant $\chi=0°$ with continuous rotation of the sample with 2θ ranging from 40° to 85°, both 10M and 14M fundamental structure reflections are found in the plot of intensity versus 2θ (Fig. 4). The lattice parameters calculated from these 10M and 14M fundamental structure reflections, using the pseudotetragonal and pseudo-orthorhombic unit cells, are $a_{14M}=6.11(3)$ Å, $b_{14M}=5.79(3)$ Å, and $c_{14M}=5.51(3)$ Å, and $a_{10M}=b_{10M}=5.91(2)$ Å and $c_{10M}=5.58(2)$ Å which is within the range of values reported in the literature.[7,20,21]

The texture scans (Ω versus 2θ, Fig. 5) performed with tilting the sample in the χ range from 0° to 90° and constant 2θ confirm the presence of 10M and 14M in the $\chi=0°$ plane. These texture scans also show at least one 10M or one 14M fundamental structure reflection in all other χ orientations except for $\chi=40°$. The broad scattering peak for $\chi=60°$ and the shadow seen for $\chi=90°$ were caused by the sample holder and are artifacts of the experimental setup. The 10M and 14M fundamental structure reflections shown in Fig. 5 were labeled and used for the texture analysis only if at least two {440} reflections were visible with similar Ω. Otherwise, a misidentification between 10M or 14M was possible and such reflections were excluded from further analysis. However, these reflections indicate that there are more grains in the foam then those identified in this analysis. The texture analysis of the (404) peaks in Fig. 6 is limited to the clearly identified 10M and 14M fundamental (404) reflections. Disregarding orientations resulting from twinning, four 10M grains (indicated with squares) and two 14M grains (indicated with triangles) were unequivocally identified and they are numbered on the χ-Ω orientation map in Fig. 6. Two fundamental structure reflections (i.e., reflection 2 at $\chi=73°$, $\Omega=51°$ and reflection 4 at $\chi=22°$, $\Omega=90°$) span over a large χ range of 9° and 12°, respectively, while the other reflection span only over a 2°–4° range. Integrating the (404) reflections of the six clearly identified grains and comparing their volume with the sum of all six grain (404) reflections, grain 2 (10M) had the largest volume fraction of 38%. Grain 3 (10M) followed with 20%, grain 5 (14M) with 19%, grain 1 (10M) with 10%, grain 4 (10M) with 8%, and grain 6 (14M) with 5%.

The polycrystalline nature of the sample was also confirmed optically during its actuation in a 0.97 T magnetic field. Several surface regions of the sample deformed differ-

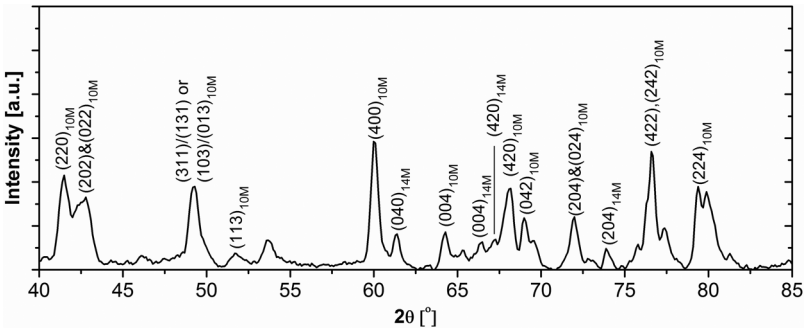

FIG. 4. 2θ neutron diffractogram of the foam sample. The sample was continuously rotated around its longest axis ($\chi=0°$). The indexes "10M" and "14M" indicate diffraction peaks that belong to 10M and 14M fundamental structure reflections.

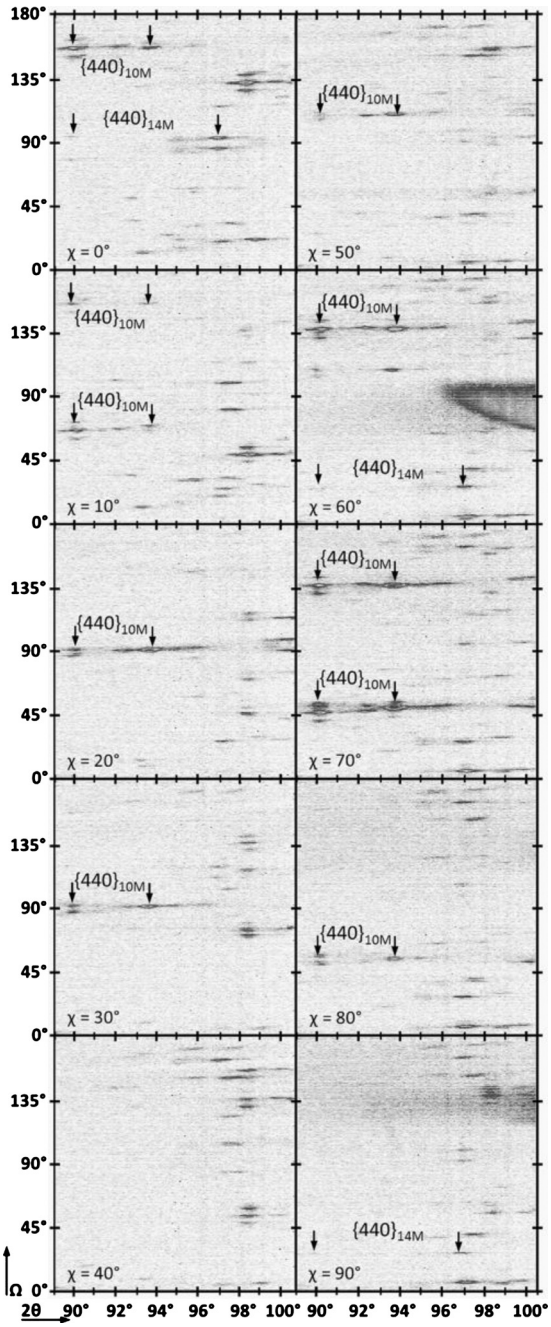

FIG. 5. $2\theta-\Omega$ neutron diffractograms of the foam sample for each χ step. Each $2\theta-\Omega$ point of the diffractogram represents the sum over a range of $\pm 5°$ of the χ value indicated. Only the 10M and 14M (specified by the subscript) fundamental reflections of grains that were identified by two {440} type reflections are indicated in the figure.

ently. By superimposing two video frames taken for mutually orthogonal magnetic field orientations (Fig. 7), the change in the distances between pores was measured with IMAGEJ (image analysis software) yielding a range of MFIS from 0.9 to $1.2\% \pm 0.1\%$ within this particular region of the sample.

Figure 8 shows the three compressive stress-strain curves of the sample where the stress, $\sigma_{\text{ext. sample}}$, is calculated using the external dimensions of the foam sample. The left ordinate shows the nominal stress, calculated as the load divided by the sample cross-section. The right ordinate shows an estimate of the stress on the metallic struts, σ_{porosity},

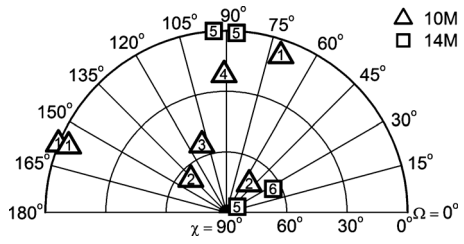

FIG. 6. χ-Ω orientation map showing the six identified 10M (△) and 14M (□) grains, labeled 1–6. Repeated labels are due to symmetry or twinning.

calculated by dividing the nominal stress by $(1-p)$, where the porosity p is 62%. All stresses mentioned here, are referring to the porosity-corrected stress. During the first compressive loading with no applied magnetic field, the sample deformed by approximately 2.1%, while the stress continuously increased up to 6 MPa. About 0.1% of this deformation was recovered elastically during unloading. During the second loading to the same maximum stress, the sample deformed approximately 0.6%, which is—taking into account the elastic recovery of 0.1%—an increment of 0.5% with respect to the value at the maximum stress during the first loading. Upon subsequent unloading in a 1 T magnetic bias field parallel to the y direction, the sample recovered a strain of 0.8%. During the third load/unload cycle, both carried out with a magnetic bias field of 1 T parallel to the y direction, the sample accrued a strain of 0.9% on loading and recovered 0.95% upon unloading. While the stress-strain curves for deformation without magnetic bias field were fairly linear during both loading and unloading, most of the deformation upon loading and unloading in a magnetic bias field took place at stresses below 1.5 MPa. In fact, during the unloading of the second deformation cycle, most of the recovery was at stresses below 0.5 MPa.

Figure 9(a) shows the sample magnetization in a magnetic field of 0.1 T as a function of the orientation of the magnetic field vector in the y-z plane. The angles 0° and 90° mark the directions of the z and y axes, respectively. The magnetization reaches a maximum value at 7°, which marks the direction of easy magnetization and a minimum at 97°, which marks the direction of hard magnetization. Figure 9(b) shows the magnetization curves along these two directions of easy and hard magnetization. In Fig. 9(b), the magnetic field is corrected for the demagnetization factor. The magnetic anisotropy energy (area between the easy and hard magnetization curves) was calculated as 41 kJ/m^3 (where the volume was corrected for porosity), which is about 20% of the anisotropy energy of single crystals.[20,22] The saturation magnetization was 62.3 $\text{A m}^2/\text{kg}$ which coincides well with reported values of single crystals.[20] The magnetization curves in the easy and hard magnetization direction were not linear (like in single crystals) but their slope monotonically decreased until saturation was reached.[7]

IV. DISCUSSION

The distribution of pore sizes throughout the sample was bimodal, with small pores subdividing all struts and nodes created by the large pores (Fig. 3). A few cracks are present,

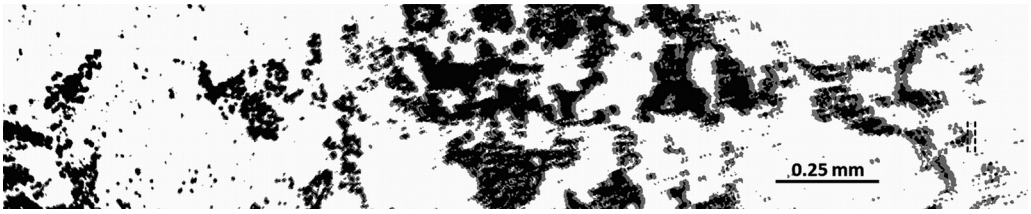

FIG. 7. Two superimposed video frames for the foam sample in a rotating magnetic field. The magnetic field direction of the two frames was perpendicular. The frames are arranged such that the top left corner regions exactly coincide. The larger the distance from this region the more the superimposed images shift apart. Two dashed lines on the right indicate the deformation from one frame to the other.

produced in a previous series of tests where the sample was subjected to 260 000 magnetomechanical cycles with MFIS values between 0.2% and 8.7%.[16] These cracks connect a few small pores and terminate in pores. Thus, it appears that pores inhibit crack growth and make the Ni–Mn–Ga foam more damage tolerant than single crystals, in which cracks grow through the entire sample.[6] Thus, porous MSMA are expected to perform better and more consistently over large numbers of actuation cycles than single crystalline MSMA.

As identified with neutron diffraction, the foam sample consists of at least six differently oriented grains (Figs. 5 and 6). The intensities diffracted from these grains indicate that they are fairly large, with a volume estimated at 1–10 mm^3, given the sample volume of 43 mm^3. Comparing the integrated intensities of the clearly identified reflections shows that grain 2 (10M) is the largest identified grain, contributing 38% of the total intensity which was correlated with individual grains. The four grains with 10M structure contribute three quarters of the identified intensity and the two grains with 14M structure one quarter. Several reflections, for which no second symmetry equivalent partner was identified, were not considered for the grain analysis. However, these reflections still demonstrate the presence of additional large grains. Furthermore, if small grains exist, they did not create enough intensity and were not detected. In conclusion, six large grains were identified in the sample, and there probably exist four more large grains and an unknown number of small grains. The sample can thus be considered polycrystalline.

The saturation magnetization of 62.3 A m^2/kg and the lattice parameters and superlattice reflections demonstrate that the chemical $L2_1$ order is well established in the austenite phase and twinning is thus likely to occur at low stresses in the martensite phase. For a polycrystalline alloy with random orientation, there should be no magnetic anisotropy (besides the shape anisotropy). The magnetic anisotropy energy of 41 kJ/m^3 (where the magnetic field was corrected for the demagnetizating field, i.e., for shape anisotropy) indicates that the foam sample is not truly randomly textured, for which the magnetic properties should be isotropic. However, with only 20% of the magnetocrystalline anisotropy energy of a single crystal, the magnetic properties (saturation curve and anisotropy energy) confirm that the net magnetic anisotropy is the result of different contributions of many grains, as expected for a polycrystalline sample.

This sample displayed previously a very large MFIS of 8.7% at 15 °C in a rotating magnetic field after thermomagnetomechanical training.[16] This value is close to the theoretical limit of 10% of single crystals with 14M structure[23] and clearly exceeds the theoretical limit of 6% of single crystals with 10M structure.[3] The orientation distribution of the grains and the large volume fraction with 10M structure indicate that magnetic-field-induced twin boundary motion can

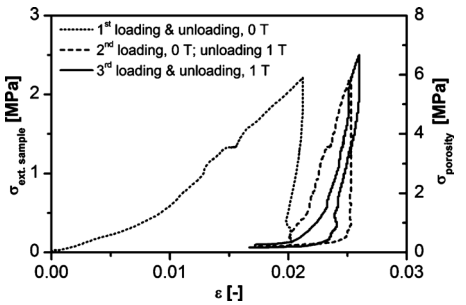

FIG. 8. Compressive loading/unloading stress-strain curves of the foam sample during static magnetomechanical test with a cross-head displacement rate of 0.125 mm/min parallel to the sample's *z*-axis. The first load/unload cycle was performed without magnetic field. During the second loading cycle, the sample was mechanically loaded without magnetic field, but unloaded in the 1 T magnetic field in *y* direction. The third load/unload cycle was performed within this 1 T magnetic field.

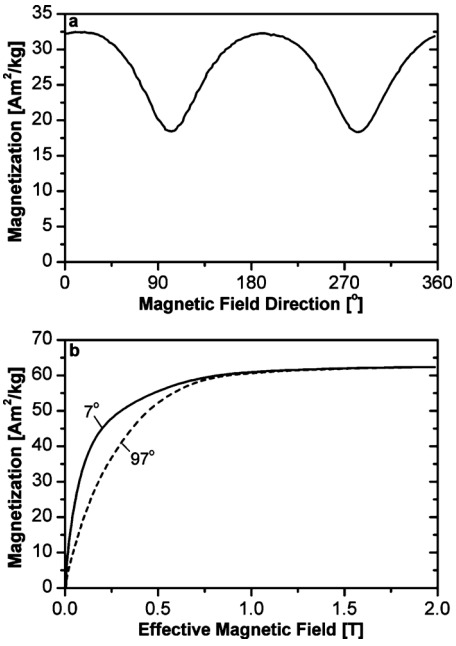

FIG. 9. Magnetization measurements of the foam sample. (a) shows the magnetization at an external magnetic field of 100 mT and rotated around the sample's shortest axis (*x* axis). (b) Magnetization curves in the easy (7°) and hard (97°) magnetization directions [as identified in (a)]. In (b) the demagnetization of the sample in different directions is taken into account.

account only partially for the large MFIS. A significant fraction of the MFIS must result from a different mechanism, which might be plastic hinging. The increased χ range of reflections 2 and 4 might be an indication for bending of those two grains supporting the hinging mechanism as proposed in Ref. 16.

An analysis of photographs taken at different field angles shows that different regions of the sample deform in different directions and with different strengths. In bulk polycrystalline MSMAs such strain incompatibilities would result in crack initialization at grain boundaries and finally to the failure by fracture. Here, the pores screen the stresses of the strain mismatch, even if grains span over more than a single strut or node, and provide a mechanism to overcome internal constraints.

In compression, foam tends to deform by plastic hinging of struts near nodes, by plastic bending of struts or by strut fracture.[24] Strains accommodated through these mechanisms would not recover in a magnetic bias field. As shown in Fig. 8, the recovery of compressive strains on the second unloading when the biasing field is present is much higher than when it is absent during the first unloading. This demonstrates that deformation occurs via twinning. These results further imply that MSMA foam may be used in actuation mode to do mechanical work against an external load.

When loading a third time under the biasing field, the yield stress was significantly lower than for the preceding, second loading experiment without field (dashed line in Fig. 8). The yield stress reduction represents a mechanical training effect, which was also found for bulk single crystalline samples[25,26] and for highly textured polycrystalline samples.[10] A training effect was previously demonstrated for the same foam sample, when thermomagnetomechanically cycled in a rotating magnetic field.[16] While deformation in a rotating magnetic field may partially be due to plastic hinging, this mechanism cannot recover the compressive strain in the current experiment in an orthogonal magnetic field. Rather, plastic hinging induced by the orthogonal field would further produce compressive strain.

V. CONCLUSIONS

A polycrystalline Ni–Mn–Ga foam with bimodal pore size distribution, for which a MFIS of up to 8.7% was previously measured,[16] was studied in detail. The hypothesis that pores effectively reduce internal constraints (due to grain boundaries) in polycrystalline Ni–Mn–Ga and external constraints (due to fixtures) in poly- and monocrystalline samples, thus enhancing (and in some cases enabling) magnetoplasticity by twinning, is substantiated by the following main results:

(1) The foam contains at least six randomly oriented millimeter-size grains with both 10M and 14M symmetry determined by neutron diffraction.
(2) The foam exhibits a homogenous pore distribution for both size ranges, with small pores inhibiting crack growth which can thus improve the performance in dynamical loading.
(3) Twinning contributes to a large portion of the magnetically induced strains in the foam, as determined by *in situ* optical observation.
(4) During a first compressive load/unload cycle, a strain of 2% is accumulated on loading by twinning, and only a very small value ($<0.1\%$) is recovered on unloading due to elastic recovery.
(5) During a second loading, an additional 0.6% strain is accumulated by twinning. Subsequent unloading under an orthogonal magnetic bias field of 1 T leads to recovery of 0.8% by reverse twinning which is enhanced by the field.
(6) For a third load/unload cycle performed with the orthogonal magnetic bias field, twinning occurs on both loading (where 0.9% strain is accumulated) and on unloading (where 0.95% strain is recovered).

ACKNOWLEDGMENTS

The authors thank Phil Boysen (Boise State University) for assistance with experimental design and machining, and Adrian Rotherbühler (Boise State University) for the setup of the optical attachment of the magnetomechanical experiment. M.C., C.W., P.M., X.Z., and D.C.D. acknowledge financial support of the National Science Foundation, Division of Materials Research Grant Nos. DMR-0804984 (BSU) and DMR-0805064 (NU). M.C. acknowledges financial support of the German Research Foundation (DFG) through the priority program SPP 1239 (Grant No. Schn 1106). P.M. is thankful to ETH Zürich, Switzerland, for donating magnetomechanical testing devices.

[1] P. Müllner, V. A. Chernenko, M. Wollgarten, and G. Kostorz, J. Appl. Phys. **92**, 6708 (2002).
[2] K. Ullakko, J. K. Huang, C. Kantner, R. C. O'Handley, and V. V. Kokorin, Appl. Phys. Lett. **69**, 1966 (1996).
[3] S. J. Murray, M. Marioni, S. M. Allen, R. C. O'Handley, and T. A. Lograsso, Appl. Phys. Lett. **77**, 886 (2000).
[4] P. Müllner, V. A. Chernenko, and G. Kostorz, J. Appl. Phys. **95**, 1531 (2004).
[5] M. Chmielus, V. A. Chernenko, W. B. Knowlton, G. Kostorz, and P. Müllner, Eur. Phys. J. Spec. Top. **158**, 79 (2008).
[6] M. Chmielus, V. A. Chernenko, A. Hilger, G. Kostorz, P. Müllner, and R. Schneider, Proceedings of ICOMAT 2008, Santa Fe, NM, June 29–July 5 2010, p. 683.
[7] M. Chmielus, *Composition, Structure and Magneto-Mechanical Properties of Ni–Mn–Ga Magnetic Shape-Memory Alloys* (Logos Verlag, Berlin, 2010).
[8] U. Gaitzsch, S. Roth, B. Rellinghaus, and L. Schultz, J. Magn. Magn. Mater. **305**, 275 (2006).
[9] M. Pötschke, U. Gaitzsch, S. Roth, B. Rellinghaus, and L. Schultz, J. Magn. Magn. Mater. **316**, 383 (2007).
[10] U. Gaitzsch, M. Pötschke, S. Roth, B. Rellinghaus, and L. Schultz, Scr. Mater. **57**, 493 (2007).
[11] M. Pötschke, S. Weiss, U. Gaitzsch, D. Cong, C. Hürrich, S. Roth, and L. Schultz, Scr. Mater. **63**, 383 (2010).
[12] U. Gaitzsch, M. Pötschke, S. Roth, B. Rellinghaus, and L. Schultz, Acta Mater. **57**, 365 (2009).
[13] D. C. Dunand and P. Müllner, "Size effects on magnetic actuation in Ni-Mn-Ga shape-memory alloys," Adv. Mater. 10.1002/adma.201002753.
[14] N. Scheerbaum, O. Heczko, J. Liu, D. Hinz, L. Schultz, and O. Gutfleisch, New J. Phys. **10**, 073002 (2008).
[15] Y. Boonyongmaneerat, M. Chmielus, D. C. Dunand, and P. Müllner, Phys. Rev. Lett. **99**, 247201 (2007).
[16] M. Chmielus, X. X. Zhang, C. Witherspoon, D. C. Dunand, and P. Müllner, Nature Mater. **8**, 863 (2009).
[17] P. Müllner, X. X. Zhang, Y. Boonyongmaneerat, C. Witherspoon, M.

Chmielus, and D. C. Dunand, Mater. Sci. Forum **635**, 119 (2010).
[18]R. C. Wimpory, P. Mikula, J. Šaroun, T. Poeste, Junhong Li, M. Hofmann, and R. Schneider, Neutron News **19**, 16 (2008).
[19]P. Müllner, V. A. Chernenko, and G. Kostorz, Scr. Mater. **49**, 129 (2003).
[20]A. Sozinov, A. A. Likhachev, and K. Ullakko, IEEE Trans. Magn. **38**, 2814 (2002).
[21]C. Jiang, Y. Muhammad, L. Deng, W. Wu, and H. Xu, Acta Mater. **52**, 2779 (2004).
[22]O. Heczko and L. Straka, J. Appl. Phys. **94**, 7139 (2003).
[23]A. Sozinov, A. A. Likhachev, N. Lanska, and K. Ullakko, Appl. Phys. Lett. **80**, 1746 (2002).
[24]L. J. Gibson and M. F. Ashby, *Cellular Solids: Structure and Properties*,2nd edition, (Cambridge University Press, Cambridge, 1997).
[25]L. Straka, O. Heczko, and H. Hänninen, Acta Mater. **56**, 5492 (2008).
[26]M. Chmielus, K. Rolfs, R. Wimpory, W. Reimers, P. Müllner, and R. Schneider, Acta Mater. **58**, 3952 (2010).